An improved method for quantifying soil aggregate stability

Ayush J. Gyawali[1], Ryan D. Stewart[1]

[1]*Department of Crop and Soil Environmental Science, Virginia Tech, Blacksburg, VA 24061*

*corresponding author: ryan.stewart@vt.edu

CORE IDEAS

We propose a metric that integrates aggregate stability measured using laser diffraction across size classes

The indicator accounts for underlying particle size differences and can differentiate micro- and macro-scale aggregates

This integrated indicator shows high correlation with traditional wet sieving methods ($R^2 \geq 0.5$)

By quantifying percent aggregated particles, the metric can be used to compare different soils

KEYWORDS: soil health; soil structure; tillage; no-till; agriculture; soil physics

ABSTRACT

Soil aggregate stability influences many biophysical and agronomic processes while acting as a key soil health indicator, yet current quantification methods suffer shortcomings including lack of repeatability, inadequate control over input energy, and inaccuracies in coarse-textured soils or those with multi-modal size distributions. In response, we propose a new method deemed integrated aggregate stability (IAS) to interpret aggregate stability using a laser diffraction machine. This method corrects for underlying particle size distributions and provides a comprehensive metric of aggregate stability. As verification, we presented repeatability tests that demonstrate the precision of the IAS method, and then compared IAS measurements to wet sieving results for three different soils. Overall, IAS showed higher correlation with the wet sieving method (R^2 = 0.49 to 0.59) than the median aggregate size (d50), which represents the most common current method for quantifying aggregate stability (R^2 = 0.09 to 0.27). Further, IAS can estimate the proportions of macro (> 0.25 mm) and micro (< 0.25 mm) aggregates, and thereby quantify shifts between those fractions under different applied energy levels. As an example, we compared IAS estimates of macro- and micro-aggregates from three different soils that due to differences in texture and previous land use showed varying levels of aggregation. While d50 identified some of the between-site differences in macro-aggregation, only IAS was able to consistently detect and quantify micro-aggregate fractions. Altogether, these results reveal that IAS can convey more consistent and relevant information about aggregate stability compared to traditionally used metrics.

INTRODUCTION

Soil aggregate stability influences biological activity and crop productivity by facilitating the movement of air and water (Amézketa, 1999; Karami et al., 2012) and by reducing soil erosive and crusting potentials (Le Bissonnais and Arrouays, 1997; Amézketa, 1999). Among other factors, the size of an aggregate affects its stability, with larger aggregates typically having lesser stability than smaller aggregates (Dexter, 1988; Six et al., 2004). For this reason, aggregates are often functionally grouped into micro- versus macro-aggregates, with a diameter of 0.25 mm used to distinguish between them (Tisdall and Oades, 1982; Amézketa et al., 2003; Fristensky and Grismer, 2008). Most aggregate stability studies have focused on the macro-aggregate fraction, as these larger units tend to reflect soil structure and soil organic matter content, while also showing greater sensitive to disturbance (Sparling et al., 1994; Boix-Fayos et al., 2001; Six et al., 2004; An et al., 2010). Despite receiving relatively little attention, micro-aggregates can act as a carbon reservoir within the soil, making their stability an important factor in carbon sequestration (Skjemstad et al., 1990; Six et al., 2000). Thus, it is important to consider both size fractions when assessing soil aggregate stability.

Due to its influence on crop productivity, as well as its rapid response to changes in management practices (Mulumba and Lal, 2008; Laghrour et al., 2016), aggregate stability has become commonly used as an indicator of soil health (Arias et al., 2005; Allen et al., 2011). Still, there exists an overall lack of consensus in how to appropriately quantify that property, with different methods typically showing low correlation to one another (Regelink et al., 2015; Almajmaie et al., 2017). A related complication arises because, even though it is often treated as constant, aggregate stability varies with the amount of applied stress (Amézketa et al., 2003). In the field, soils are subjected to various levels of energy, particularly near the soil surface, with light

rainfall representing an example of low applied energy (Shin et al., 2016) and vehicle traffic representing high applied energy (Ungureanu et al., 2017). Some studies have attempted to connect this energy input with the breakdown of aggregates (Mayer et al., 2011; Schomakers et al., 2015), but there is still little consistency in how such methods are applied and interpreted (Almajmaie et al., 2017).

Aggregate stability is typically measured using one of two general approaches: mechanical sieving or laser diffraction. Sieving can be done with wet or dry aggregates, using either a single sieve (e.g., to capture the 1-2 mm size fraction) or nested sieves (Kemper and Rosenau, 1986). Using a single sieve allows for determination of a mass fraction known as percentage of stable aggregates (Yoder, 1936; De Leenheer and De Boodt, 1959), while nested sieves can be used to calculate mean weight diameter (MWD), geometric mean diameter (GMD), and proportion of stable aggregates (Yoder, 1936). Sieve-based measurements suffer from several drawbacks, including a lack of repeatability, inadequate ability to quantify or regulate input energy, limited number of sieve sizes, and bias towards larger aggregates sizes (Tisdall and Oades, 1982; Amézketa, 1999; Rawlins et al., 2013). In an attempt to address the first two drawbacks, researchers have explored using ultrasound waves (i.e., sonication) as a way to control the energy applied to the aggregates (Mentler et al., 2004). Even with such modifications, sieving has limited capability to resolve micro-aggregate fractions.

Laser diffraction measurements can detect a wider distribution of aggregate sizes, though these data are typically summarized using only the median size (d50). Aggregate stability can then be described by analyzing shifts in d50 under different applied energy levels (Bieganowski et al., 2010; Virto et al., 2011; Rawlins et al., 2013). While d50 has the advantage of being a single number, thus allowing comparison between different treatments and/or applied energy levels, it

does not account for textural differences between soils. In contrast, the corrected d50 ($d50_c$) corrects for the particle size distribution of the sample, and is calculated as (Rawlins et al., 2013):

$$d50_c = d50 - d50_{psd} \quad [1]$$

where $d50_{psd}$ represents the median particle size. Still, $d50_c$ may not capture shifts between macro and micro aggregates, or even between aggregates and individual particles, particularly when applied to coarse-textured soils such as sands.

To overcome the shortcomings associated with current methods to quantify aggregate stability, we propose a new indicator deemed integrated aggregate stability (IAS). This indicator accounts for all aggregates < 2 mm in size, allows for controlled energy inputs, and corrects for the underlying particle size distribution of the soil. Further, IAS can be set to differentiate between micro- and macro-aggregates, allowing quantification of the dynamics of these fractions under different applied energies. Given its ability to consistently and accurately detect aggregate stability across size classes, the IAS method should serve as a standard by which to quantify and compare aggregate stability.

THEORY

Integrated aggregate stability (IAS)

The cumulative size distribution function measured by a laser diffraction machine, $F(x)$, represents the integral of the measured density function, $f(x)$:

$$F(x) = \int_0^x f(s)ds \quad [2]$$

In the integrated aggregate stability (IAS) method, the cumulative distribution functions are measured for independent samples representing aggregated soils (hereafter "*a*") and dispersed samples composed of individual particles (hereafter "*p*"), such that:

$$F_a(x) = \int_0^x f_a(s)ds \quad [3]$$

$$F_p(x) = \int_0^x f_p(s)ds \quad [4]$$

$F(x)$ and $f(x)$ both represent relative volume fractions, with the former scaled between 0 and 1. However, due to the presence of internal porosity, aggregate formation often increases the specific volume of the soil, V, where V = volume of soil/mass of soil. In other words, a given mass of soil will have greater volume when its particles are aggregated as opposed to when they are dispersed. The total volume per mass of dispersed particles, $V_{t,p}$ [L^3 M^{-1}], and aggregated particles, $V_{t,a}$ [L^3 M^{-1}], can be used to convert the relative volume density functions into volume-corrected density functions, $v(x)$:

$$v_a(x) = V_{t,a} \cdot f_a(x) \quad [5]$$

$$v_p(x) = V_{t,p} \cdot f_p(x) \quad [6]$$

Likewise, we can combine Equations [3] and [5], and also Equations [4] and [6], to obtain the volume-corrected cumulative distribution functions for aggregates (V_a) and particles (V_p):

$$V_a(x) = V_{t,a}\int_0^x f_a(s)ds = V_{t,a}F_a(x) \quad [7]$$

$$V_p(x) = V_{t,p}\int_0^x f_p(s)ds = V_{t,p}F_p(x) \quad [8]$$

The two volume-corrected density functions, $v_a(x)$ and $v_p(x)$, will cross at some value x_1:

$$v_p(x_1) = v_a(x_1) \quad [9].$$

Further, because aggregation causes an overall shift of the volume distribution towards larger particle sizes, we can assume:

$$V_p(x_1) - V_a(x_1) = \int_0^{x_1} \left(v_p(s) - v_a(s)\right)ds \geq 0 \quad [10].$$

For the entire range of particle/aggregate sizes ($0 < x \leq x_{max}$), the aggregated sample will have equal or higher specific volume than the dispersed particles, meaning that:

$$V_{t,p} - V_{t,a} = V_p(x_{\max}) - V_a(x_{\max}) = \int_0^{x_{\max}} \left(v_p(s) - v_a(s)\right)ds \leq 0 \quad [11].$$

Equation [11] can also be written as:

$$V_{t,p} - V_{t,a} = \int_0^{x_1} \left(v_p(s) - v_a(s)\right)ds + \int_{x_1}^{x_{\max}} \left(v_p(s) - v_a(s)\right)ds \quad [12].$$

Equation [12] can be rearranged as:

$$\int_{x_1}^{x_{\max}} \left(v_a(s) - v_p(s)\right)ds = V_{t,a} - V_{t,p} + \int_0^{x_1} \left(v_p(s) - v_a(s)\right)ds \quad [13].$$

We now define the integrated aggregate stability, IAS, as (Figure 1):

$$\text{IAS} = \frac{1}{V_{t,a}} \int_{x_1}^{x_{\max}} \left(v_a(s) - v_p(s) \right) ds \qquad [14].$$

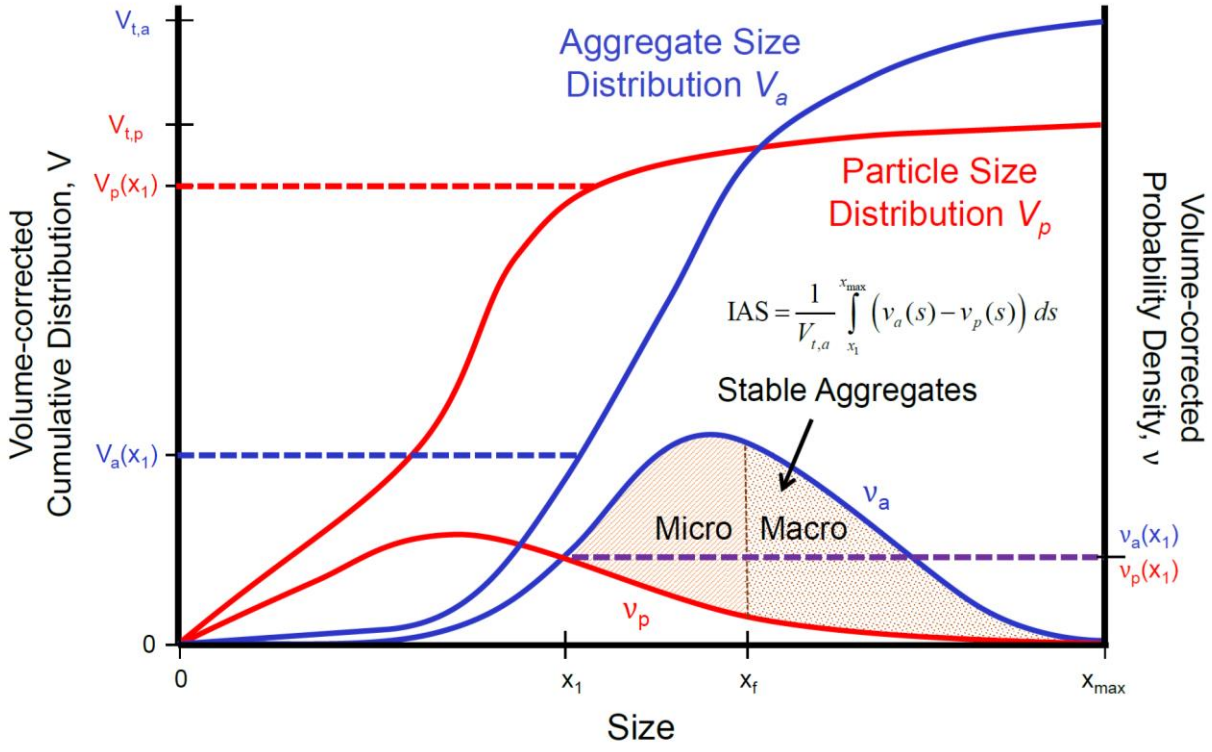

Figure 1 – Schematic showing the integrated aggregate stability (IAS) metric, which is calculated as the area between the volume-corrected aggregate and particle density functions, respectively $v_a(x)$ and $v_p(x)$, over the range of diameters between x_1 and x_{max}.

Combining the Equations [13] and [14] we obtain:

$$\text{IAS} = 1 - \frac{V_{t,p}}{V_{t,a}} + \frac{1}{V_{t,a}} \int_{0}^{x_1} \left(v_p(s) - v_a(s) \right) ds \qquad [15].$$

We will use the symbol λ to define the ratio of specific volumes as:

$$\lambda = V_{t,p} / V_{t,a} \quad [16].$$

Substituting Equation [16] into Equation [15]:

$$\mathrm{IAS} = 1 - \lambda + \lambda F_p(x_1) - F_a(x_1) \quad [17].$$

Bi- or multi-modal particle size distributions

Some soils, particularly coarse-textured ones, may have multiple crossings where the volume-corrected density functions $v_p(x)$ and $v_a(x)$ have identical values. We will call these crossings x_1, x_2, $x_3 \ldots x_N$, noting that $v_p(x)$ and $v_a(x)$ will have an odd number of crossings so long as the dispersed particles are smaller in size than the aggregated samples. In the case of a bimodal particle size distribution with three crossings, we can rewrite Equation [12] as:

$$V_{t,p} - V_{t,a} = \int_0^{x_1} \left(v_p(s) - v_a(s)\right) ds + \int_{x_1}^{x_2} \left(v_p(s) - v_a(s)\right) ds + \int_{x_2}^{x_3} \left(v_p(s) - v_a(s)\right) ds + \int_{x_3}^{x_{\max}} \left(v_p(s) - v_a(s)\right) ds \quad [18].$$

IAS in this instance will be defined as:

$$\mathrm{IAS}_{\mathrm{bimodal}} = \frac{1}{V_{t,a}} \int_{x_1}^{x_2} \left(v_a(s) - v_p(s)\right) ds + \frac{1}{V_{t,a}} \int_{x_3}^{x_{\max}} \left(v_a(s) - v_p(s)\right) ds \quad [19].$$

Substituting Equations [16] and [19] into Equation [18] yields:

$$\mathrm{IAS}_{\mathrm{bimodal}} = 1 - \lambda + \lambda F_p(x_1) - \lambda F_p(x_2) + \lambda F_p(x_3) - F_a(x_1) + F_a(x_2) - F_a(x_3) \quad [20].$$

Using the same approach, Equation [20] can be generalized for any multi-modal distribution as:

$$\mathrm{IAS}_{\mathrm{multimodal}} = 1 - \lambda + \lambda \sum_{\substack{i=1 \\ i \text{ odd}}}^{N} F_p(x_i) - \lambda \sum_{\substack{i=2 \\ i \text{ even}}}^{N-1} F_p(x_i) + \sum_{\substack{i=2 \\ i \text{ even}}}^{N-1} F_a(x_i) - \sum_{\substack{i=1 \\ i \text{ odd}}}^{N} F_a(x_i) \quad [21].$$

Separation between micro- and macro-aggregates

We will use x_f to represent the size fraction chosen to separate micro- versus macro-aggregates (e.g., 0.25 mm). In the case that the crossing point of the volume-weighted particle and aggregate density functions (x_1) is smaller than x_f, we can rewrite Equation [12] as:

$$V_{t,p} - V_{t,a} = \int_0^{x_1} \left(v_p(s) - v_a(s)\right) ds + \int_{x_1}^{x_f} \left(v_p(s) - v_a(s)\right) ds + \int_{x_f}^{x_{\max}} \left(v_p(s) - v_a(s)\right) ds \quad [22].$$

We can then define the micro-aggregate stability, IAS_{micro}, as:

$$IAS_{micro} = \frac{1}{V_{t,a}} \int_{x_1}^{x_f} \left(v_a(s) - v_p(s)\right) ds \quad [23].$$

Substituting Equations [16] and [23] into [22], we obtain:

$$IAS_{micro} = \lambda F_p(x_1) - \lambda F_p(x_f) + F_a(x_f) - F_a(x_1) \quad [24].$$

Likewise, we can define the macro-aggregate stability, IAS_{macro}, as:

$$IAS_{macro} = \frac{1}{V_{t,a}} \int_{x_f}^{x_{\max}} \left(v_a(s) - v_p(s)\right) ds \quad [25]$$

$$IAS_{macro} = 1 - \lambda + \lambda F_p(x_f) - F_a(x_f) \quad [26].$$

Quantification of dispersive energy applied to the soil

During measurements of aggregated samples, ultrasonic energy may be applied. The total ultrasonic energy density applied to the soil suspension, J_s [E L^{-3}], can be estimated as:

$$J_s = P_s t_s / \upsilon_s \quad [27]$$

where P_s is the applied power [E t^{-1}], t_s is the time over which sonication was applied [t], and υ_s is the volume of the ultrasonic chamber [L^3].

Using an energy balance, North (1976) quantified the fraction of applied energy consumed in dispersing the soil aggregates, β, as:

$$\beta = E_s / P_s t_s \quad [28]$$

where E_s represents the ultrasonic energy adsorbed in dispersing soil [E].

Rearranging the full energy balance, β can be calculated as:

$$\beta = \left[1 - \frac{\Delta T'}{\Delta T}\left(1 + \frac{m_{sa} c_s}{m_w c_w + w_v}\right)\right] \cong 1 - \frac{\Delta T'}{\Delta T} \quad [29]$$

where $\Delta T'$ is the change in temperature [T] of the soil and water suspension, ΔT is the change in temperature [T] for pure water under the same applied energy (Pt), m_{sa} is the mass of air dry soil [M], c_s is the specific heat of soil [E M^{-1} T^{-1}], m_w is mass of water [M], c_w is the specific heat of water [E M^{-1} T^{-1}] and w_v is the thermal capacity of the chamber [E T^{-1}].

MATERIALS AND METHODS

Soil descriptions

To demonstrate the IAS method and compare its estimated aggregate stability values with those estimated by other laser diffraction metrics (i.e., d50 and $d50_c$) and by wet seiving, we collected and analyzed soil samples from three locations. The first set of samples (deemed Site 1 hereafter) came from Blacksburg, Virginia, 6 km west of the Virginia Tech campus (37°12'25.3"N 80°29'12.0"W) in a long term no-till corn field. The soil was a silt loam composed of the Duffield-Ernest-Purdy undifferentiated group: Duffield - *Fine-loamy, mixed, active, mesic Ultic Hapludalfs*; Ernest - *Fine-loamy, mixed, superactive, mesic Aquic Fragiudults*; Purdy - *Fine,*

194 *mixed, active, mesic Typic Endoaquults* (NRCS, 2017). Soil samples were taken from the surface
195 (0-5 cm) layer in April 2016 with sixteen physical replicates collected (i.e., n = 16). A second set
196 of surface samples were also collected in September 2016 (n = 16). The mean organic carbon
197 content for these soils was 3.8 g kg^{-1} dry soil (n = 16).

198 The second set of soils (Site 2) came from a research farm in Ferrum, Virginia (36°55'13.6"N,
199 80°02'15.5"W). The soil was a silt loam classified as a Bluemount-Spriggs-Redbrush complex:
200 Bluemount - *Fine-loamy, mixed, superactive, mesic Typic Hapludalfs*; Spriggs - *Fine-loamy,*
201 *mixed, active, mesic Ultic Hapludalfs*; Redbrush - *Fine, mixed, superactive, mesic Typic*
202 *Hapludalfs*. The soil had been in long-term grazed pasture before the grass was terminated in
203 September 2015. The soil samples were collected in April 2016 from the 0-5 cm surface layer (n
204 = 16). The mean organic carbon content for these soils was 6.2 g kg^{-1} dry soil (n = 16).

205 The third set of soils (Site 3) were collected near Blackstone, Virginia (37°05'44.0"N,
206 77°57'40.1"W), in a field that transitions between Appling (*Fine, kaolinitic, thermic Typic*
207 *Kanhapludults*) and Durham (*Fine-loamy, siliceous, semiactive, thermic Typic Hapludults*) sandy
208 loam soils (NRCS, 2017). The field was initially planted in fescue that was terminated in
209 September 2015. In April 2016, soil samples were taken from the surface (0-5 cm) layer (n = 16).
210 The mean organic carbon content for these soils was 2.6 g kg^{-1} of dry soil (n = 16).

211 *Aggregate stability quantification*

212 Particle size and aggregate size distributions were measured using a CILAS 1190 laser
213 diffraction (LD) machine with a built-in 25 W ultrasound unit (CILAS Inc., Orleans, France).
214 During analysis, samples were subjected to one of four applied energy levels: 1) 0 J ml^{-1}, where
215 no sonication was applied; 2) 0.5 J ml^{-1}, where 13 seconds of sonication was applied; 3) 1 J ml^{-1},
216 where 26 seconds of sonication was applied; and 4) 5 J ml^{-1}, where 130 seconds of sonication

was applied. For each run, soil was added to the LD machine until the sample obscurance reached 3-4%, at which time sonication was applied to the specified energy level. After the application of specified energy, the total measurement time to quantify $F_p(x)$ or $F_a(x)$ was ~3 minutes. To obtain particle size distributions, 0.2 grams of each sample was taken and mixed with a suspension of 1 ml sodium hexametaphosphate (5%) and 4 ml of DI water. This mixture was shaken on reciprocating shaker on low setting for 4 hours. The mixture was added to the LD machine and sonicated for 130 seconds before its size distribution was recorded.

After obtaining the aggregate and particle size distributions, aggregate stability was analyzed using d50 and the proposed method, IAS (Equation [17] or [20], depending on the nature of each sample). The samples collected in April 2016 from Sites 1-3 were also evaluated for IAS_{micro} (Equation [24]) and IAS_{macro} (Equation [26]) with x_f = 0.25 mm (n = 16 per site). λ was assumed to equal 0.75 for all IAS calculations, as discussed in the following subsection.

Evaluation of the relative specific volume parameter λ

The IAS indicator requires an estimate for λ, which represents the specific volume of dispersed particle relative to those same particles when aggregated (i.e., Equation [16]). If the particles are spheres or ellipsoids of varying sizes, theoretical packing ratios suggest λ values of 0.64 to 0.74 (Donev et al., 2004; Kyrylyuk and Philipse, 2011). For example, a sample composed to two different sphere sizes would have a λ value of ~0.74 (O'Toole and Hudson, 2011). Using laboratory measurements, Currie (1966) showed that λ varied between 0.69 and 0.79 for a variety of air-dried agricultural soils. For purposes of this study we assumed λ to equal 0.75, as this represents an average measured value also supported by theory.

To better understand the potential error associated with assuming a constant value for λ, we performed a sensitivity analysis using two soils from Site 1 and two from Site 3. IAS was

estimated using Equation [17], assuming λ = 0.2, 0.5, 0.7, 0.9 and 1.0. Parameter sensitivity ratio (S_r) was then calculated as (Hamby, 1994):

$$S_r = \frac{I_o(O_m - O_0)}{O_o(I_m - I_0)} \quad [30]$$

where I_o is the original parameter input (assumed for this analysis to be λ = 0.7), I_m is the modified parameter input, O_o is the original output (i.e., the calculated IAS value with λ = 0.7) and O_m is the IAS output with the modified parameter input.

Accuracy and precision of measurements

LD accuracy was stated by the manufacturer to be ± 3 x 10^{-3} mm; we verified this accuracy using polystyrene size standards of 10^{-4}, 10^{-3}, 0.01, and 0.1 mm (Sigma-Aldrich, Inc., St. Louis, USA). For each physical replicate analyzed on the LD machine, we ran two separate subsamples to check for measurement precision. So long as the two runs had higher precision than the LD machine accuracy, the first measurement was retained for subsequent analysis.

As a demonstration of the repeatability of LD-generated data, we homogenized a sample from Site 1 and another sample from Site 3, and then took four subsamples from each sample. The subsamples were then split for analysis within the LD machine under no sonication (0 J ml^{-1}) and 0.5 J ml^{-1} sonication, with another portion dispersed for particle size analysis. The resulting cumulative distribution data, $F(x)$, were plotted as mean values plus 95% confidence intervals.

Wet aggregate stability quantification

We investigated the relationship between the proposed IAS indicator, along with d50 (the traditional LD indicator), with water stable aggregation measured by wet sieving (Kemper and Rosenau, 1986). Samples were taken from Sites 1-3 (n = 32 for Site 1, representing the two

sampling times there, and n = 16 for Sites 2 and 3). All samples were air-dried and then gently sieved to 4 mm. Subsamples were then passed through a 2 mm sieve for LD analysis, since the laser diffraction machine used in this analysis was limited to sizes < 2.5 mm. The LD analysis was run on all subsamples with no applied sonication (0 J ml^{-1} applied energy) and 13 seconds of applied sonication (0.5 J ml^{-1}). The particle size distribution was also measured for each subsample.

For the wet sieving, we placed 50 g of air-dry sample on top of nested sieves with openings of 2, 0.25, and 0.053 mm, with a collection tray on the bottom. This setup was lowered into water and submerged for 5 minutes. After 5 minutes, we vertically oscillated the sieves 50 times by hand. The soil remaining in each sieve was dried and weighed and corrected for small pebbles and sand content. The proportion of water stable aggregates 0.053 to 4 mm in size was calculated as a sum of the water stable aggregates collected in the 0.053, 0.25, and 2 mm sieves, divided by the total dry mass of the sample.

Results from the three LD indicators (d50, $d50_c$, and IAS) were independently compared to the < 4 mm wet seive fraction using linear regression.

Dispersive energy quantification

To determine the fraction of dispersive energy consumed by the soil aggregates, β (Equation [29]), we measured ΔT using pure water, and $\Delta T'$ using suspension of soil plus water. The applied ultrasonic power P_s was fixed at 25 W, while the time of sonication was fixed at 130 seconds.

RESULTS

Examples of cumulative distribution functions, $F(x)$, and probability density functions, $f(x)$, for two soils are shown in Figure 2. The first soil, from Site 2, was a fine-textured silt loam, and its size distribution consistently shifted to smaller sizes as the amount of applied ultrasonic energy increased (Figure 2a). The second soil, from Site 3, was a coarse-textured sandy loam. While the aggregated sample with no applied sonication (0 J ml^{-1}) had a unimodal distribution, the samples analyzed with higher ultrasonic energies (0.5, 1, and 5 J ml^{-1}) and as dispersed particles (psd) showed bimodal distributions (Figure 2b). Whereas the standard IAS equation (Equation [17]) was used to analyze the soil from Site 2, the samples from Site 3 required use of $IAS_{bimodal}$ (Equation [20]).

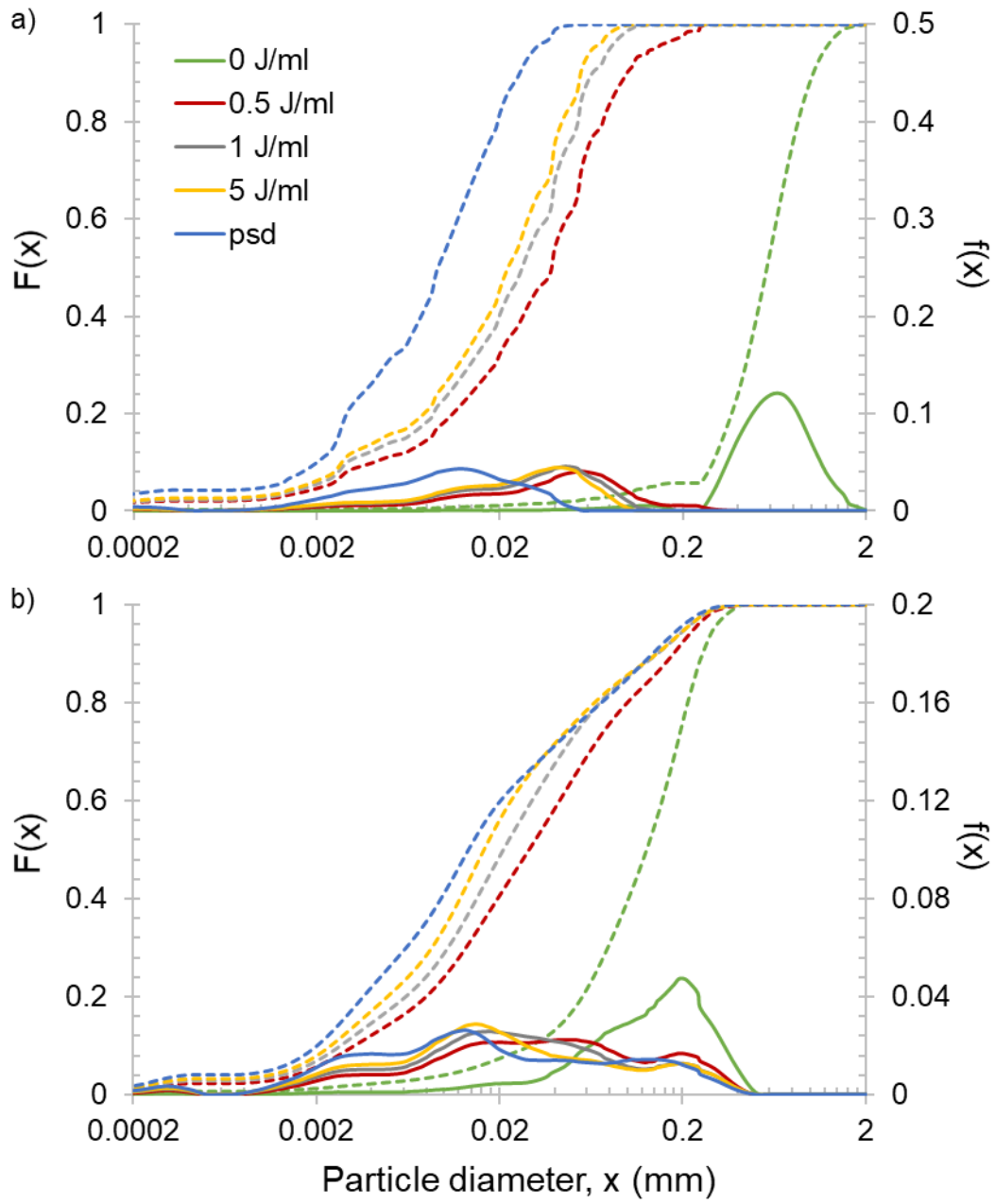

Figure 2 – Examples of cumulative distributions, $F(x)$, and probability densities, $f(x)$, for soils from a) Site 2, and b) Site 3. Four different ultrasonic energies were applied to each set of soils: 0, 0.5, 1, and 5 J ml^{-1}; the underlying particle size distributions were also measured (psd). Solid lines show probability density functions, $f(x)$, and dotted lines show cumulative distribution functions, $F(x)$.

298 The repeatability test conducted on samples from Sites 1 and 3 showed that data generated from
299 the laser diffraction (LD) machine had high precision (Figure 3). Further, applying ultrasonic
300 energy to the samples caused consistent shifts in aggregate size distributions, as seen by the
301 narrow confidence intervals for both soils with no sonication (0 J ml^{-1}) versus 13 seconds of
302 sonication (0.5 J ml^{-1}). This consistency in quantifying aggregate and particle size distributions
303 indicated that the LD machine provides repeatable measurements for aggregate and particle size
304 distributions.

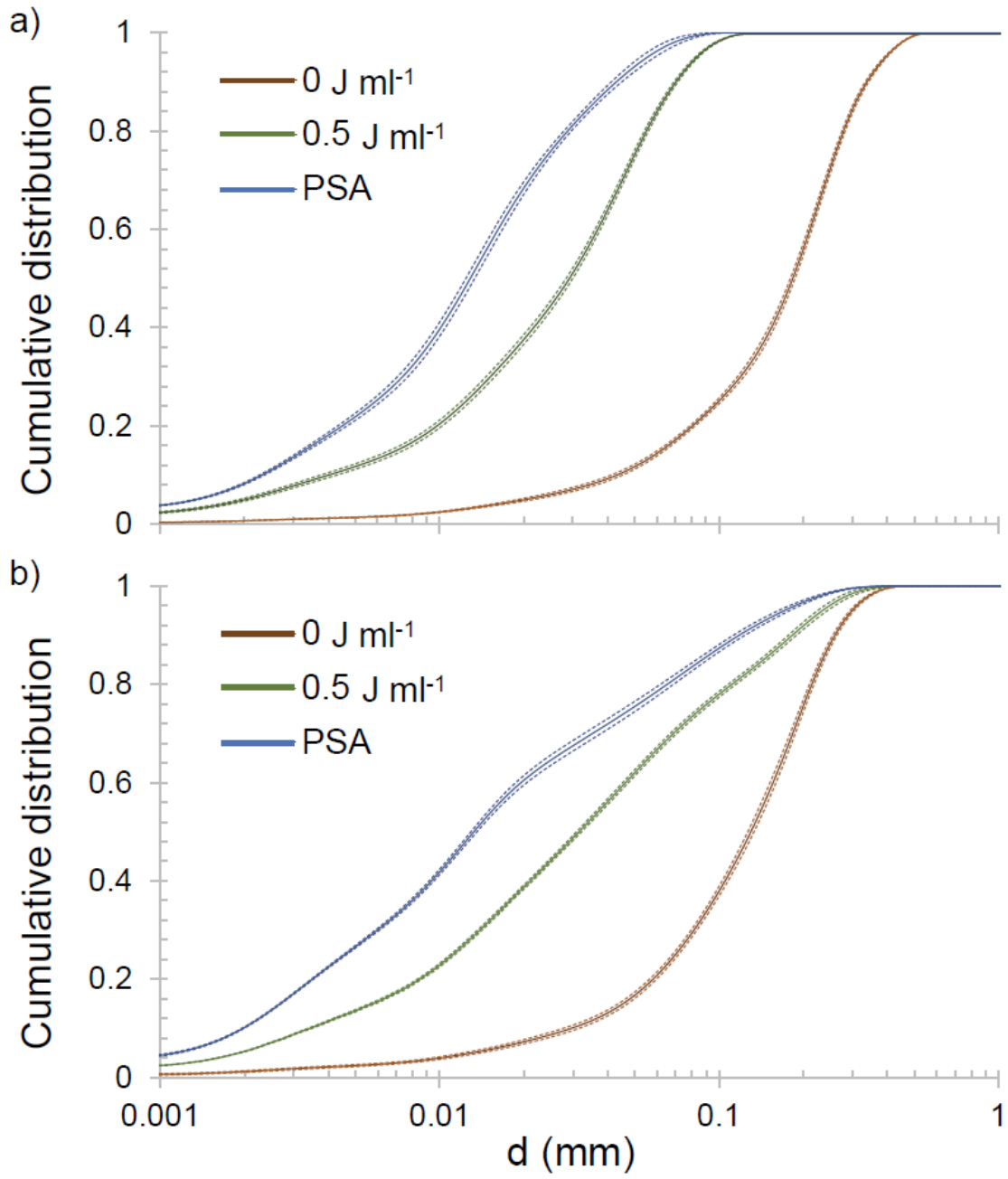

Figure 3 – Repeatability test for cumulative distribution functions generated by laser diffraction measurements for two samples from a) Site 1, and b) Site 3. Four replicates of each sample were analyzed with no dispersion or applied sonication (0 J ml^{-1}), no dispersion with 13 seconds of sonication (0.5 J ml^{-1}), and full dispersion (particle size). Solid lines indicate mean values for each size class; dashed lines represent 95% confidence intervals.

The proposed integrated aggregate stability (IAS) indicator requires an estimate of the relative specific volumes of the dispersed versus aggregated particles (λ; Equation [16]). As revealed by the sensitivity analysis, IAS has an inverse linear relationship with λ (Figure 4). Smaller λ values downscale the volume-corrected probability density function for the dispersed particles, $v_p(x)$, meaning that the aggregated particles will represent a higher proportion of the total aggregate sample as λ decreases. The four soils had mean sensitivity ratio S_r values (Equation [30]) that ranged from -0.49 to -0.075. Site 3 (sandy loam soil) had greater sensitivity to λ than Site 1 (silt loam soil), suggesting that coarse-textured soils may be more sensitive to λ than fine-textured soils.

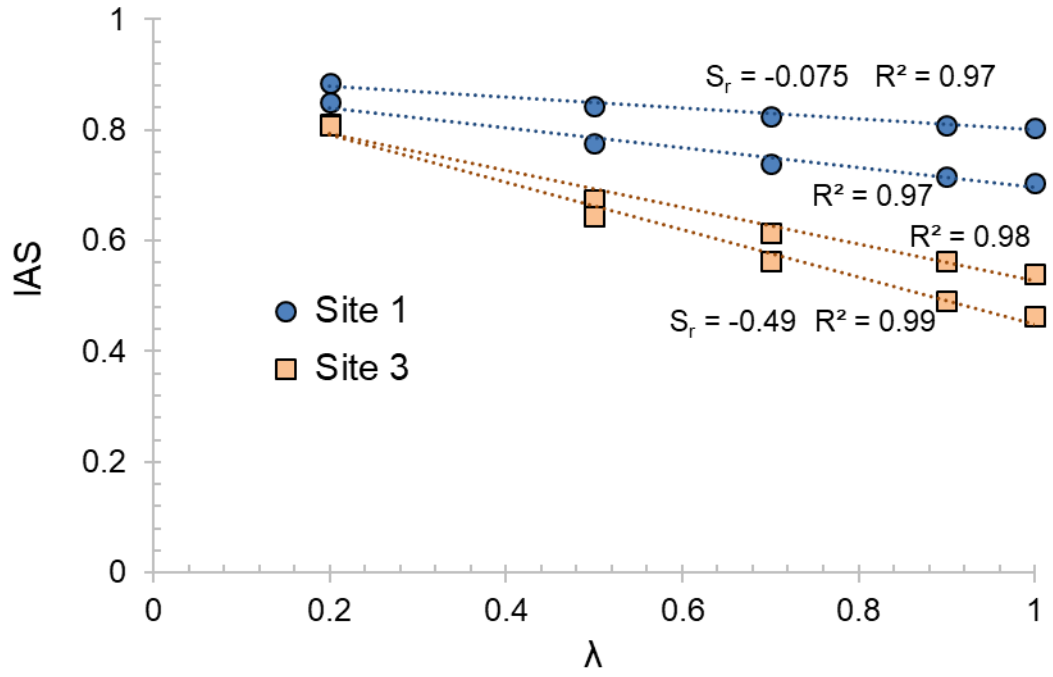

Figure 4 – Sensitivity analysis of integrated aggregate stability (IAS) with the specific volume correction factor λ for two samples from Site 1 (blue and yellow points) and two samples from Site 3 (orange and gray points).

Near-surface soil samples collected from Sites 1-3 (n = 32 for Site 1 and n = 16 for Sites 2 and 3) were analyzed via LD and wet sieving (presented here as the proportion of total sample mass represented by water stable aggregates 0.053 – 4 mm). With no applied sonication (0 J ml^{-1}), the LD measurements as analyzed by IAS showed positive correlation with the wet sieving results (R^2 = 0.59; Figure 5a). The LD measurements with the input energy of 0.5 J ml^{-1} also showed relatively good correlation with the sieve-generated data when analyzed using IAS (R^2 = 0.49; Figure 5b). In contrast, the d50 metric traditionally used to interpret LD data showed low correlation with the wet sieving results (R^2 = 0.27 for 0 J ml^{-1} ultrasonic energy and R^2 = 0.09 for 0.5 J ml^{-1} applied energy; Figures 5c and 5d). The corrected $d50_c$ values (Equation [1]) had the same correlations with the wet sieving data as d50 (R^2 = 0.27 for 0 J ml^{-1} ultrasonic energy and R^2 = 0.09 for 0.5 J ml^{-1} applied energy; data not shown).

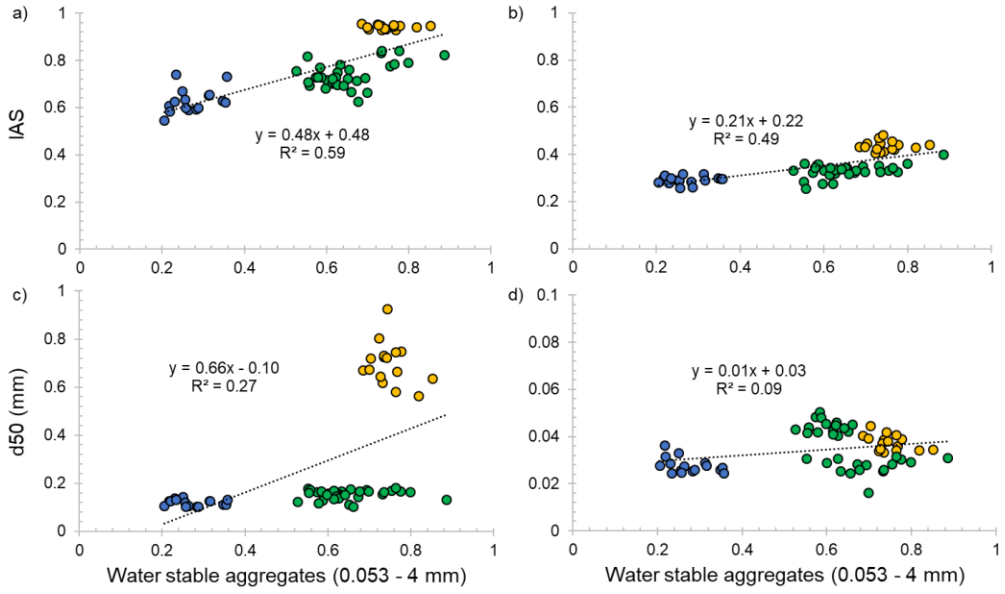

Figure 5 – Relationship between water stable aggregates measured using wet sieving (values are presented as a proportion of total sample mass) versus integrated aggregate stability (IAS) for a) 0 J ml^{-1} and b) 0.5 J ml^{-1}; or versus median aggregate size d50 for c) 0 J ml^{-1} and d) 0.5 J ml^{-1}. Green points represent Site 1, yellow points represent Site 2, and blue points represent Site 3.

The soils from Sites 1-3 were also evaluated for IAS, IAS_{micro}, and IAS_{macro} under no sonication and the three applied ultrasonic energy densities (n = 16 per site and energy level). Site 2 had the highest IAS values for all energy densities, while Site 3 had the lowest IAS values (Figure 6a). When the aggregates were analyzed without sonication (0 J ml^{-1}), Site 2 primarily contained macro-aggregates > 0.25 mm in size. The application of ultrasonic energy dispersed most of the macro-aggregates from all three sites, though Site 2 retained some macro-aggregates at the 0.5 J ml^{-1} energy level. Site 3 (coarse-textured loamy sand) had non-zero values for IAS_{macro} at all applied energy levels, which may represent aggregates that formed around relatively large sand particles. Still, Site 3 had lower IAS values than the other two sites (fine-textured silt loams).

The LD measurements were also analyzed using d50 and $d50_c$ (Figure 6b), which both showed that Site 2 had greater aggregate stability than the other two sites at 0 J ml^{-1}. All sites had $d50/d50_c$ values < 0.05 mm for the other applied energy densities.

The quantification of dispersive energy contributing to soil aggregate breakdown showed that an average of 36 ± 11% of the applied ultrasonic energy was consumed in dispersing the soil aggregates (data not shown). Taking the applied energy levels of 0.5, 1, and 5 J m^{-1}, the soil aggregates experienced true dispersive energy levels of approximately 0.2, 0.4, and 2 J ml^{-1}.

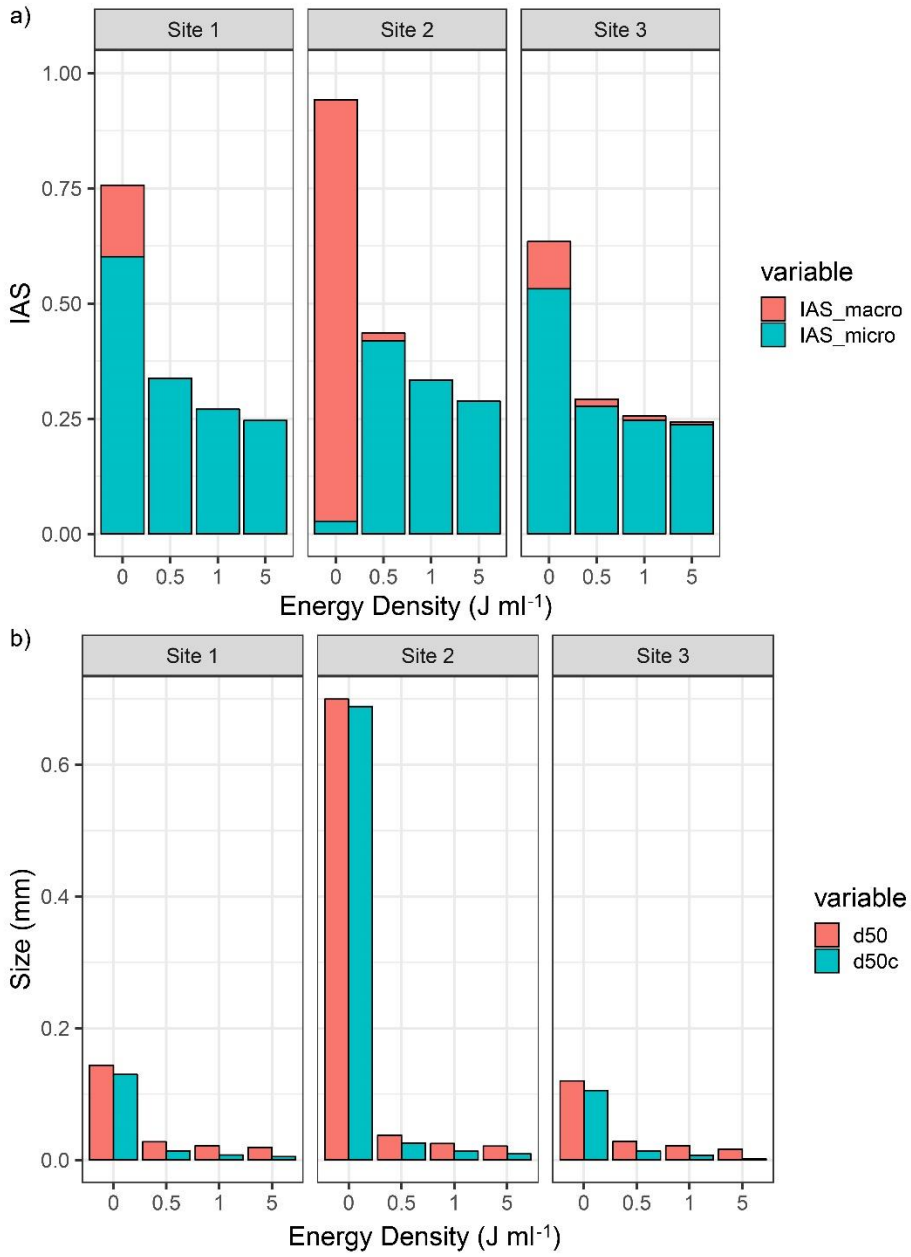

Figure 6 – Laser diffraction measurements for soils from three sites and four applied sonication energies, 0, 0.5, 1, and 5 J ml^{-1}, as analyzed using a) IAS, including relative proportions of micro-aggregates IAS_{macro} (Equation [24]) and macro-aggregates IAS_{macro} (Equation [26]), and b) median aggregate size d50 and median aggregate size corrected for median particle size $d50_c$. Note that 0.25 mm was used to separate micro- from macro-aggregates, and that the figures show mean values from n = 16 replicates per site and applied energy.

DISCUSSION AND CONCLUSION

In this paper we presented a new indicator that can quantify soil aggregate stability using laser diffraction (LD) measurements. In general, aggregate stability measurements using laser diffraction can overcome many of the shortcomings of traditional sieve methods, such as lack of repeatability, inability to quantify applied energy, and limited size range of aggregates that can be measured. Still, LD measurements have primarily been analyzed using median particle sizes (d50 or $d50_c$; Equation [1]). In contrast, our proposed integrated aggregate stability (IAS) indicator provides an estimate of the overall percentage of aggregates versus individual particles, e.g., an IAS value of 0.80 indicates that at least 80% of the total volume of the aggregated samples is made up of aggregates. At the same time, IAS had higher correlation with wet sieving data compared to the d50 and d50c indicators (Figure 5). As wet sieving represents a widely used method for determining aggregate stability (Kemper and Rosenau, 1986; Regelink et al., 2015; Almajmaie et al., 2017), the correlation shown here suggests that LD measurements may capture some of the same information when interpreted by IAS. Further, because the IAS presents LD data as a percentage of aggregated particles, it may be possible to set threshold values that can convey if a soil is resistant to aggregate breakdown, e.g., the 70% water stable aggregate threshold used by Amézketa et al. (2003).

In its standard form (Equation [17]), IAS quantifies all aggregates < 2 mm in size, meaning that it integrates macro- and micro-aggregates together. Still, the IAS framework retains the capability to distinguish between micro-aggregate stability (IAS_{micro}; Equation [24]) and macro-aggregate stability (IAS_{macro}; Equation [26]). This flexibility means that IAS can quantify how soil aggregates shift between macro- and micro-aggregate fractions at different levels of dispersive energy. As an example, we caclulated IAS, IAS_{micro}, and IAS_{macro}, for three different

386 soils that differed in both their overall level of aggregation and in the distributions between
387 macro and micro-aggregates (Figure 6). In this specific example, Site 2, which was a fine-
388 textured silt loam soil that had previously been in pasture, had higher overall IAS values than
389 Site 1 (silt loam in continuous row crop cultivation) or Site 3 (coarse-textured sandy loam
390 previously in pasture). When the samples were analyzed without applied sonication (0 J ml^{-1}),
391 Site 2 also showed a substantially higher proportion of aggregates within the macro-aggregate
392 fraction, whereas most of the aggregates in Sites 1 and 3 existed within the micro-aggregate
393 fraction. This result may be because Site 2 had higher organic carbon content (6.2 g kg^{-1}) than
394 Site 1 (3.8 g kg^{-1}) or Site 3 (2.6 g kg^{-1}). The d50 and $d50_c$ metrics also reflected relative amounts
395 of macro-aggregation at each site (i.e., higher $d50/d50_c$ for Site 2 compared to Sites 1 and 3 for 0
396 J ml^{-1}); however, those metrics proved incapable of differentiating between sites at higher levels
397 of applied ultrasonic energy. The $d50/d50_c$ indicators therefore showed limited ability to detect
398 micro-sized aggregates that were present in these soils. Taken altogether, these results reveal that
399 IAS represents a superior option to study dynamics of different aggregate fractions when
400 working with LD measurements, and demonstrate the potential for IAS_{macro} and IAS_{micro} to
401 capture textural and land use effects on aggregation.

402 One primary advantage of LD measurements is that the amount of energy applied to the
403 aggregates can be quantified (Mayer et al., 2011; Schomakers et al., 2015). Still, these
404 calculations can suffer from some uncertainties. For example, while we focused our energy
405 density calculations on the energy applied via the ultrasonic unit, the stirrer and pumps of the
406 unit will also impart energy on the suspension (as detailed in the Appendix). There also exists
407 uncertainty when translating these applied energies to those forces that a field soil might face.
408 For example, a rainstorm with an intensity of 25 mm h^{-1} and a duration of 1 hour translates to an

409 energy density of approximately 0.1 J ml^{-1} if absorbed by the top 0.5 cm of soil (Shin et al.,
410 2016). The lowest applied ultrasonic energy (0.5 J ml^{-1}, translating to 0.2 J ml^{-1} of dispersive
411 energy) thereby approximates the dispersive force of a typical heavy rainfall when quantified in
412 volumetric terms, i.e., [E L^{-3}]. However, because of the dilute concentration of soil aggregates
413 within the ultrasonic chamber (~0.001 g ml^{-1}), the corresponding energy densities on a
414 gravimetric [E M^{-1}] basis were higher than those experienced by typical field soils. For example,
415 assuming 1 g of soil was added to the ultrasonic chamber (which here had a volume of ~650 ml),
416 the aggregates could have experienced more than 1000 J g^{-1} at the highest applied energy level.
417 This value is two orders of magnitude larger than typical rainfall intensities (e.g., ~10 J g^{-1};
418 North, 1976); as a result, users should apply care when deciding whether to quantify energy
419 inputs on a volumetric or gravimetric basis.

420 Another source of uncertainty in the IAS procedure resides in the λ parameter, which was used to
421 account for specific volume differences between aggregated versus dispersed particles. In the
422 calculations performed here, we assumed $\lambda = 0.75$, which represents a mean value supported by
423 particle packing theory and experimental measurements of intra-aggregate porosity. To evaluate
424 the effect of assuming a constant λ value, we performed a sensitivity analysis (S_r; Equation [30]).
425 The four tested samples had mean values of $-0.5 \leq S_r \leq -0.075$. Previous studies have suggested
426 that $|S_r| \leq 0.5$ or ≤ 1.0 represents a model parameter with low or damped sensitivity (Chaves,
427 2009; Gloe, 2011), meaning that the IAS calculation will be somewhat insensitive to the exact
428 value of λ. Still, IAS accuracy will increase as λ becomes better constrained, particularly in
429 coarse-textured soils, where the particle size and aggregate size distributions may have
430 substantial overlap (i.e., $f_p(x)$ and $f_a(x)$ curves with similar shapes). At the same time, we
431 assumed a constant λ regardless of applied energy, though in reality λ will likely increase as the

aggregated samples become more dispersed into individual particles (e.g., with the 1 and 5 J ml^{-1} ultrasonic energies). Numerous experimental procedures can be used to estimate the specific volume of aggregates, including measuring displacement when aggregates are added to non-wetting or non-mixing fluids (McIntyre and Stirk, 1954; Sarli et al., 2001), or estimating aggregate volume using three-dimensional scanners (Sander and Gerke, 2007) or image reconstruction (Stewart et al., 2012). Particle specific volumes can be estimated using pycnometers (Klute et al., 1986). Thus, future work may therefore build on these methods to better constrain λ, and by extension improve the accuracy of IAS.

In conclusion, the integrated aggregate stability (IAS) indicator provides the ability to better interpret LD measurements, as it quantifies the total proportion of aggregated particles within a sample. Based on 64 samples collected from 3 sites, IAS showed relatively high correlation with water stable aggregation measurements collected by the wet sieving method ($R^2 \geq 0.5$). Further, IAS can be modified to quantify relative percentages of macro and micro aggregates within a sample. This capability means that future studies can better analyze soil resistance to failure under various applied stresses, which ultimately can be used to quantify and predict soil resilience. Based on these advantages, we conclude that IAS is altogether an improved method for quantifying soil aggregate stability.

APPENDIX – Quantification of stirrer and pump energies

The power input into a suspension by a stirring paddle, E_p [E], can be estimated as:

$$E_p = P_p t_p \quad [A1]$$

where P_p [E t^{-1}] is the power of the stirring paddle and t_p [t] is the time that the stirrer is operated.

The stirrer power can be estimated from the drag force of the paddle and the mean velocity of the stirrer paddle. Under the assumption that the mean stirrer velocity is 0.75 times the velocity at the end of the stirrer (Logan, 2012), E_p can be estimated as:

$$E_p = \frac{0.75^3}{2} b_{d,p} A_p \rho_w \omega^3 r_p{}^3 t_p \qquad [A2]$$

where $b_{d,p}$ [-] is the paddle drag coefficient, A_p [L^2] is the cross-sectional area of the paddle, ρ_w [M L^{-3}] is the density of water, ω [L L^{-1} t^{-1}] is the angular velocity and r_p [L] is the radius of the paddle. For a paddle with a length-to-width ratio of 5, $b_{d,p}$ is ~1.2, while the maximum possible value of $b_{d,p}$ is 1.9 (Logan, 2012).

The CILAS 1190 laser diffraction unit used in this experiment has values related to the stirrer of A_p = 7.2 x 10^{-4} m^2, r_p = 0.029 m, ω = 36.6 rad s^{-1}. For 240 seconds of stirring and assuming $b_{d,p}$ = 1.2 and ρ_w = 1000 kg m^{-3}, the applied energy E_p is ~50 J. The total volume of suspension in the laser diffraction system is 620 ml, giving an energy density from the stirrer of 0.08 J ml^{-1}.

The pumping of the fluid also imparts energy to the suspension, due to friction losses within the tubing. The work applied by the pump, W_f [E], can be found as:

$$W_f = \Delta p \upsilon_t \qquad [A3]$$

where Δp is the pressure drop within the tubing [M L^{-1} t^{-2}] and υ_t [L^3] is the total volume of the flow system, made up of tubing plus mixing chamber. Provided that the flow system and pump represent a closed system, the work provided by the pump is equal to the energy absorbed by the suspension, E_f [E]. If we assume that the mixing chamber has a negligible contribution to the total volume and friction losses of the flow system, we can calculate the pressure drop in the tubing per unit length using the Darcy-Weisbach equation:

$$\frac{\Delta p}{L} = f \frac{\rho_w u_f^{\,2}}{2D_t} \qquad [A4]$$

where f [-] is a friction factor, D_t [L] is the diameter of the tubing, and u_f [L t^{-1}] is the velocity of the fluid.

The volume of tubing is equal to the area of tubing multiplied by the tubing length L_t [L], i.e., $\upsilon_{tubing} = \pi/4\ D_t^2 L_t$. Further, the total pressure drop depends on the total distance that the fluid has traveled, L_d [L], which is equal to the fluid velocity multiplied by the duration of pumping, t_d [t], i.e., $L_d = u_f t_f$. Assuming $\upsilon_t \approx \upsilon_{tubing}$, we can use these relationships in Equations [A3] and [A4] to obtain the energy associated with friction losses in the flow system:

$$E_f = f \frac{\pi \rho_w L_t D_t u_f^{\,3} t_d}{8} \qquad [A5].$$

The flow system of the unit also has values of L_t = 3.68 m, D_t = 6.4 x 10^{-3} m, u_f = 0.54 m s^{-1}. The Reynolds number is found by Re = $\rho_w u_f D_t/\mu$, where μ [M L^{-1} t^{-1}] is the dynamic viscosity of water (assumed here to equal 9 x 10^{-4} kg m^{-1} s^{-1}). For these flow conditions, Re = 3.84 x 10^3, which assuming a smooth pipe translates to a fraction factor of $f \approx 0.04$ (Brown, 2003). For 240 seconds of pumping, the applied energy E_f is ~14 J, which translates to an energy density of 0.02 J ml^{-1}. The combined energy of the pump and stirrer for four minutes is therefore ~0.1 J ml^{-1}, which represents approximately 1/5 of the energy provided by the ultrasonic unit at the lowest applied energy level (0.5 J ml^{-1}).

The limited effect of the stirrer and pump on aggregate stability measurements was verified by running an aggregated sample through the machine and collecting repeated measurements using four different homogenized subsamples. For the first subsample, the size distribution was

measured immediately after adding the sample to the machine (0 seconds). The second subsample was measured after 240 seconds of continuous stirring and pumping. For the third subsample, the ultrasonic unit, stirrer, and pump were applied for 240 seconds before measurement, and the fourth subsample was allowed to run with sonication, pump, and stirrer for 480 seconds. The resulting data show that the pump plus stirrer caused a minor shift in the aggregate size distribution, whereas the initial 240 seconds of sonication caused a much larger shift towards smaller aggregates (Figure A1). Thus, the ultrasonic unit represents the dominant means by which energy is imparted onto the aggregates in this particular system. These calculations may prove useful to other users who either lack an ultrasonic unit or wish to apply lower levels of energy than sonication can provide.

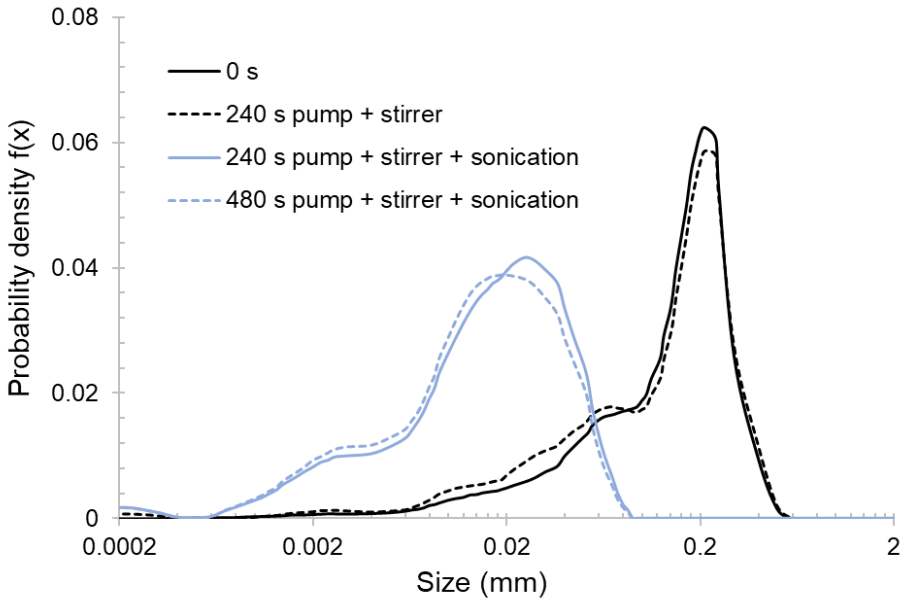

Figure A1 – Probability density functions, $f(x)$, for a soil sample from Site 2 that was analyzed immediately after addition to the laser diffraction machine (0 seconds), versus measured after: 240 seconds of pumping and stirring the sample; 240 seconds of pumping and stirring with ultrasonic; and 480 seconds of pumping and stirring with ultrasound.

510 REFERENCES

511 Allen, D.E., B.P. Singh and R.C. Dalal. 2011. Soil Health Indicators Under Climate Change: A
512 Review of Current Knowledge. In: B. P. Singh, A. L. Cowie and K. Y. Chan, editors, Soil
513 Health and Climate Change. Springer, Berlin, Germany. p. 25-45.
514 Almajmaie, A., M. Hardie, T. Acuna and C. Birch. 2017. Evaluation of methods for determining
515 soil aggregate stability. Soil and Tillage Research 167: 39-45.
516 Amézketa, E. 1999. Soil Aggregate Stability: A Review. Journal of Sustainable Agriculture 14:
517 83-151. doi:10.1300/J064v14n02_08.
518 Amézketa, E., R. Aragüés, R. Carranza and B. Urgel. 2003. Macro-and micro-aggregate stability
519 of soils determined by a combination of wet-sieving and laser-ray diffraction. Spanish
520 Journal of Agricultural Research 1: 83-94.
521 An, S., A. Mentler, H. Mayer and W.E.H. Blum. 2010. Soil aggregation, aggregate stability,
522 organic carbon and nitrogen in different soil aggregate fractions under forest and shrub
523 vegetation on the Loess Plateau, China. CATENA 81: 226-233.
524 doi:10.1016/j.catena.2010.04.002.
525 Arias, M.E., J.A. González-Pérez, F.J. González-Vila and A.S. Ball. 2005. Soil health: A new
526 challenge for microbiologists and chemists. International Microbiology 8: 13-21.
527 Bieganowski, A., M. Ryżak and B. Witkowska-Walczak. 2010. Determination of soil aggregate
528 disintegration dynamics using laser diffraction. Clay Minerals 45: 23-34.
529 Boix-Fayos, C., A. Calvo-Cases, A.C. Imeson and M.D. Soriano-Soto. 2001. Influence of soil
530 properties on the aggregation of some Mediterranean soils and the use of aggregate size
531 and stability as land degradation indicators. CATENA 44: 47-67. doi:10.1016/S0341-
532 8162(00)00176-4.

533 Brown, G.O. 2003. The history of the Darcy-Weisbach equation for pipe flow resistance.
534 Environmental and Water Resources History. p. 34-43.
535 Chaves, H.M.L. 2009. Sensibilidade do modelo Hydrus aos parâmetros hidráulicos do solo em
536 diferentes texturas. Revista Brasileira de Recursos Hídricos 14: 33-37.
537 Currie, J. 1966. The volume and porosity of soil crumbs. Journal of Soil Science 17: 24-35.
538 De Leenheer, L. and M. De Boodt. 1959. Determination of aggregate stability by the change in
539 mean weight diameter. Mededelingen van landbouwhogeschool en de opzoekingstations
540 van de staat te Gent 24: 290-300.
541 Dexter, A. 1988. Advances in characterization of soil structure. Soil and Tillage Research 11:
542 199-238.
543 Donev, A., I. Cisse, D. Sachs, E.A. Variano, F.H. Stillinger, R. Connelly, et al. 2004. Improving
544 the density of jammed disordered packings using ellipsoids. Science 303: 990-993.
545 Fristensky, A. and M.E. Grismer. 2008. A simultaneous model for ultrasonic aggregate stability
546 assessment. CATENA 74: 153-164. doi:10.1016/j.catena.2008.04.013.
547 Gloe, M. 2011. Evaluating a Process-based Mitigation Wetland Water Budget Model. M.S.
548 Thesis. Virginia Tech, Blacksburg, VA, USA.
549 Hamby, D. 1994. A review of techniques for parameter sensitivity analysis of environmental
550 models. Environmental monitoring and assessment 32: 135-154.
551 Karami, A., M. Homaee, S. Afzalinia, H. Ruhipour and S. Basirat. 2012. Organic resource
552 management: Impacts on soil aggregate stability and other soil physico-chemical
553 properties. Agriculture, Ecosystems & Environment 148: 22-28.
554 doi:10.1016/j.agee.2011.10.021.

555 Kemper, W. and R. Rosenau. 1986. Aggregate stability and size distribution. In: A. Klute, editor
556 Methods of Soil Analysis. Part 1. SSSA, Madison, WI, USA.
557 Klute, A., G. Blake and K.H. Hartge. 1986. Particle density. In: A. Klute, editor Methods of Soil
558 Analysis. Part 1. SSSA, Madison, WI, USA.
559 Kyrylyuk, A.V. and A.P. Philipse. 2011. Effect of particle shape on the random packing density
560 of amorphous solids. physica status solidi (a) 208: 2299-2302.
561 Laghrour, M., R. Moussadek, R. Mrabet, R. Dahan, M. El-Mourid, A. Zouahri, et al. 2016. Long
562 and Midterm Effect of Conservation Agriculture on Soil Properties in Dry Areas of
563 Morocco. Applied and Environmental Soil Science 2016: 9. doi:10.1155/2016/6345765.
564 Le Bissonnais, Y. and D. Arrouays. 1997. Aggregate stability and assessment of soil crustability
565 and erodibility: II. Application to humic loamy soils with various organic carbon
566 contents. European Journal of Soil Science 48: 39-48. doi:10.1111/j.1365-
567 2389.1997.tb00183.x.
568 Logan, B.E. 2012. Environmental transport processes. John Wiley & Sons, Hoboken, NJ.
569 Mayer, H., J. Schomakers, A. Mentler, N. Degischer and W.E. Blum. 2011. Measurement of soil
570 aggregate stability using low intensity ultrasonic vibration. Spanish Journal of Soil
571 Science 1(1) 8-19.
572 McIntyre, D. and G. Stirk. 1954. A method for determination of apparent density of soil
573 aggregates. Australian Journal of Agricultural Research 5: 291-296.
574 Mentler, A., H. Mayer, P. Strauß and W. Blum. 2004. Characterisation of soil aggregate stability
575 by ultrasonic dispersion. International Agrophysics 18: 39-46.
576 Mulumba, L.N. and R. Lal. 2008. Mulching effects on selected soil physical properties. Soil and
577 Tillage Research 98: 106-111. doi:10.1016/j.still.2007.10.011.

578 North, P. 1976. Towards an absolute measurement of soil structural stability using ultrasound.
579 European Journal of Soil Science 27: 451-459.
580 NRCS. 2017. Web Soil Survey. In: USDA, editor.
581 O'Toole, P.I. and T.S. Hudson. 2011. New high-density packings of similarly sized binary
582 spheres. The Journal of Physical Chemistry C 115: 19037-19040.
583 Rawlins, B., J. Wragg and R. Lark. 2013. Application of a novel method for soil aggregate
584 stability measurement by laser granulometry with sonication. European Journal of Soil
585 Science 64: 92-103.
586 Regelink, I.C., C.R. Stoof, S. Rousseva, L. Weng, G.J. Lair, P. Kram, et al. 2015. Linkages
587 between aggregate formation, porosity and soil chemical properties. Geoderma 247: 24-
588 37.
589 Sander, T. and H.H. Gerke. 2007. Noncontact Shrinkage Curve Determination for Soil Clods and
590 Aggregates by Three-Dimensional Optical Scanning. Soil Science Society of America
591 Journal 71: 1448-1454. doi:10.2136/sssaj2006.0372.
592 Sarli, G.O., R.R. Filgueira and D. Giménez. 2001. Measurement of soil aggregate density by
593 volume displacement in two non-mixing liquids. Soil Science Society of America Journal
594 65: 1400-1403.
595 Schomakers, J., F. Zehetner, A. Mentler, F. Ottner and H. Mayer. 2015. Study of soil aggregate
596 breakdown dynamics under low dispersive ultrasonic energies with sedimentation and X-
597 ray attenuation. International Agrophysics 29: 501-508.
598 Shin, S.S., S.D. Park and B.K. Choi. 2016. Universal power law for relationship between rainfall
599 kinetic energy and rainfall intensity. Advances in Meteorology 2016: 1-11.
600 doi:doi:10.1155/2016/2494681.

Six, J., H. Bossuyt, S. Degryze and K. Denef. 2004. A history of research on the link between (micro)aggregates, soil biota, and soil organic matter dynamics. Soil and Tillage Research 79: 7-31. doi:10.1016/j.still.2004.03.008.

Six, J., E.T. Elliott and K. Paustian. 2000. Soil macroaggregate turnover and microaggregate formation: a mechanism for C sequestration under no-tillage agriculture. Soil Biology and Biochemistry 32: 2099-2103. doi:10.1016/S0038-0717(00)00179-6.

Skjemstad, J., R. Lefeuvre and R. Prebble. 1990. Turnover of soil organic matter under pasture as determined by ^{13}C natural abundance. Soil Research 28: 267-276. doi:10.1071/SR9900267.

Sparling, G., P. Hart, J. August and D. Leslie. 1994. A comparison of soil and microbial carbon, nitrogen, and phosphorus contents, and macro-aggregate stability of a soil under native forest and after clearance for pastures and plantation forest. Biology and Fertility of Soils 17: 91-100.

Stewart, R.D., M.R. Abou Najm, D.E. Rupp and J.S. Selker. 2012. An Image-Based Method for Determining Bulk Density and the Soil Shrinkage Curve. Soil Science Society of America Journal 76: 1217-1221.

Tisdall, J.M. and J.M. Oades. 1982. Organic matter and water-stable aggregates in soils. European Journal of Soil Science 33: 141-163.

Ungureanu, N., V. Vlăduţ and S.Ş. Biriş. 2017. FEM modelling of soil behaviour under compressive loads. IOP Conference Series: Materials Science and Engineering, IOP Publishing.

622 Virto, I., N. Gartzia-Bengoetxea and O. Fernández-Ugalde. 2011. Role of Organic Matter and
623 Carbonates in Soil Aggregation Estimated Using Laser Diffractometry. Pedosphere 21:
624 566-572. doi:10.1016/S1002-0160(11)60158-6.
625 Yoder, R.E. 1936. A direct method of aggregate analysis of soils and a study of the physical
626 nature of erosion losses. Agronomy Journal 28: 337-351.

627